Synthesis and Structural Characterization of Iridium Clusters Formed Inside and Outside the Pores of Zeolite NaY

Fen Li and Bruce C. Gates*

Department of Chemical Engineering and Materials Science, University of California, Davis, California 95616

Received: June 25, 2003; In Final Form: August 5, 2003

Zeolite NaY-supported $Ir_4(CO)_{12}$ was prepared by direct deposition onto the outside surface of the zeolite crystals and by reductive carbonylation of $Ir(CO)_2(acac)$ sorbed in its pores. These samples and the products of their decarbonylation and subsequent recarbonylation were characterized by infrared and extended X-ray absorption fine structure spectroscopies. The data show that the clusters in the zeolite pores were molecularly dispersed and could be reversibly decarbonylated and recarbonylated, whereas those on the outer surface outside the pores were aggregated under decarbonylation condition (300 °C in He) and could not be reversibly recarbonylated. The results demonstrate stabilization of the molecular clusters entrapped in the pores.

Introduction

Highly dispersed supported metal cluster catalysts are employed in many large-scale applications, exemplified by selective naphtha reforming to make aromatics, for which the catalysts are LTL zeolites incorporating platinum clusters inferred to contain about 5−12 atoms each, on average.[1] Preparation of stable, highly dispersed metal clusters is challenging because the clusters typically aggregate, especially at high temperatures and in reactive environments. At high temperatures, metals migrate out of zeolite pores to form larger aggregates on the outer zeolite surfaces,[2] and under some conditions, metal clusters in zeolite pores grow so fast that they cause the zeolite crystallites to burst.[3] Nevertheless, zeolites have been suggested to be attractive supports because zeolite encagement of clusters could limit their movement and minimize their aggregation.[4−6] This suggestion has not been well tested.

Our goal was to test the hypothesis that zeolite entrapment stabilizes metal clusters by investigating metal clusters in and on zeolite NaY. The clusters were chosen to be $Ir_4(CO)_{12}$ and decarbonylated species formed from it. Because a molecule of $Ir_4(CO)_{12}$ is too large to fit easily through the windows connecting the supercages of zeolite NaY, it can be directly sorbed on its outer surface but not within the pores. To prepare these clusters in the zeolite pores, we used a ship-in-a-bottle synthesis of $Ir_4(CO)_{12}$ by reductive carbonylation of sorbed $Ir(CO)_2(acac)$, which easily fits in the pores.[7] The structures were characterized by infrared (IR) and extended X-ray absorption fine structure (EXAFS) spectroscopies.

Experimental Methods

Materials. Zeolite NaY was obtained from the Davison Division of W. R. Grace; the Si/Al atomic ratio was 2.6. The zeolite was initially calcined at 300 °C in flowing O_2 (Matheson Extra Dry Grade) for 4 h and evacuated at 10^{-3} Torr at the final calcination temperature for 12 h. Syntheses of metal clusters in and on the zeolite and sample transfers were performed with exclusion of air and moisture on a double-manifold Schlenk vacuum line and in a N_2-filled glovebox (AMO-2032, Vacuum Atmospheres). He and CO (99.995%) were purified by passage through traps containing particles of Cu and activated zeolite to remove traces of O_2 and moisture, respectively. *n*-Pentane (Aldrich, 99.0%) and tetrahydrofuran (THF) (Aldrich, anhydrous, 99.9%), used as solvents, were refluxed under N_2 in the presence of Na/benzophenone ketyl to remove traces of water and then deoxygenated by sparging of dry N_2 prior to use. $Ir_4(CO)_{12}$ (Strem, ≥98%), $Ir(CO)_2(acac)$ (dicarbonylacetylacetonato iridium (I), Strem, 99%), and bis-(triphenylphosphine)iminium chloride [PPN][Cl] (Aldrich, 97%) were used as received.

Sample Preparation. $Ir_4(CO)_{12}$ supported on zeolite NaY was prepared by slurrying the calcined zeolite support with $Ir_4(CO)_{12}$ in *n*-pentane for 2 days, followed by room-temperature evacuation for 1 day to remove the solvent. $Ir_4(CO)_{12}$ in the pores of the zeolite was formed by slurrying $Ir(CO)_2(acac)$ with calcined zeolite NaY in *n*-pentane for 2 days, followed by room-temperature evacuation for 1 day to remove the solvent; the resultant sample was carbonylated in flowing CO in a tubular flow reactor at 40 °C for 12 h, as described elsewhere.[7,8] The Ir content of each sample was 1.0 wt %.

Scanning Electron Microscopy (SEM). The zeolite particles were examined by high-resolution scanning electron microscopy. The instrument was an FEI XL30 SFEG (Philips XL30 with a LaB6 emission source).

IR Spectroscopy. Spectra were recorded with a Bruker IFS-66v spectrometer with a spectral resolution of 4 cm^{-1}. Samples were pressed into thin self-supporting wafers and mounted in a controlled-atmosphere cell in the glovebox. Purified He or CO flowed through the cell. Each sample was scanned 64 times, and the signal was averaged. Details of the experiments are as reported elsewhere.[7]

Attempted Extraction of Metal Carbonyls from Zeolite NaY. Attempts were made to extract iridium carbonyls from zeolite samples by contacting them with [PPN][Cl] in freshly distilled THF under N_2. The supernatant liquid was transferred by syringe into a solution IR cell and quickly scanned. The method matches those of successful extractions of iridium carbonyl species, such as have been reported for $Ir_4(CO)_{12}$ and $Ir_6(CO)_{16}$ supported on γ-Al_2O_3.[9,10] Similar attempts have failed to extract iridium carbonyl clusters and rhodium carbonyl

* To whom correspondence should be addressed.

10.1021/jp035813z CCC: $25.00
Published on Web 09/25/2003

TABLE 1: Crystallographic Data Characterizing the Reference Compounds and Fourier Transform Ranges Used in the EXAFS Data Analysis[a]

	crystallographic data			Fourier transform		
sample	shell	*N*	*R* [Å]	Δk [Å^{-1}]	Δr [Å]	*n*
Ir crystal	Ir−Ir[b]	12	2.72	0.9−19.4	1.6−3.3	1
$Na_2Pt(OH)_6$	Pt−O[c]	6	2.05	1.4−17.7	0.5−2.0	3
$Ir_4(CO)_{12}$	Ir−C[d]	3	1.87	2.8−16.5	1.1−2.0	3
	Ir−O*[d]	3	3.01	2.8−16.5	2.0−3.3	3

[a] Notation: *N*, coordination number for absorber-backscatterer pair; *R*, distance; Δk, limits used for forward Fourier transform (*k* is the wave vector); Δr, limits used for shell isolation (*r* is distance); *n*, power of *k* used for Fourier transform. [b] Crystal structure data from ref 14. [c] Crystal structure data from ref 15. [d] Crystal structure data from ref 17.

clusters from zeolites, with the results taken as evidence of entrapment of the clusters in the zeolite pores.[7,8,11]

X-ray Absorption Spectroscopy. EXAFS spectroscopy experiments were performed at X-ray beam line 4−1b at the Stanford Synchrotron Radiation Laboratory (SSRL) at the Stanford Linear Accelerator Center, Stanford, California, and at beam line X-11A at the National Synchrotron Light Source (NSLS) at Brookhaven National Laboratory, Upton, NY. The storage ring energy at SSRL was 3 GeV and the ring current was 60−100 mA; at NSLS the ring energy was 2.8 GeV and the ring current 180−280 mA. EXAFS data were recorded for wafers of each solid sample in transmission mode after the cell had been cooled to nearly liquid nitrogen temperature. The data were collected with a Si(220) or Si(111) double crystal monochromator that was detuned by 30% to minimize effects of higher harmonics in the X-ray beam. The samples were scanned at energies near the Ir L_{III} absorption edge (11215 eV). Details of the experiments are as reported.[8,11,12]

Analysis of EXAFS Data. The methods of data analysis are essentially the same as those described elsewhere.[13] The EXAFS data were analyzed with experimentally determined reference files obtained from EXAFS data characterizing materials of known structure, except that the Ir−Ir reference file was determined theoretically with the FEFF software.[14] The Ir−O support interaction was analyzed with phase shifts and backscattering amplitudes obtained from EXAFS data characterizing $Na_2Pt(OH)_6$.[15] The transferability of the phase shifts and backscattering amplitudes characterizing platinum and iridium (which are near neighbors in the periodic table) has been justified experimentally.[16] The Ir−C and Ir−O* contributions (where O* represents carbonyl oxygen) were analyzed with phase-shifts and backscattering amplitudes obtained from EXAFS data characterizing crystalline $Ir_4(CO)_{12}$, which has terminal and no bridging CO ligands.[17] The parameters used to extract these results from the EXAFS data are summarized in Table 1. The reliable parameters representing the high-*Z* (Ir) and low-*Z* contributions ($O_{support}$, CO) were determined by multiple-shell fitting in both *r* (distance) and *k* (wave vector) space with comparisons of fits and data represented with both k^1 and k^3 weightings.[18] The data quality is high, and the analysis was carried out without Fourier filtering, as described elsewhere.[19]

Results

SEM. A SEM image of zeolite NaY crystallites is presented in the Supporting Information, Figure 1. The average diameter of the particles is about 0.5 μm, assuming spherical particles.

IR Evidence of $Ir_4(CO)_{12}$ Deposited on Zeolite NaY. After contacting of $Ir_4(CO)_{12}$ in *n*-pentane with zeolite NaY for 2 days followed by evacuation to remove the solvent, the sample was characterized by IR spectroscopy. The spectrum (Figure 1a) includes ν_{CO} bands at 2116(w), 2076(s), and 2040(m, sh) cm^{-1}, resembling that of $Ir_4(CO)_{12}$ in THF solution (2109(vw), 2067-(vs), 2027(m, sh) cm^{-1}) and that of a sample made by carbonylation of zeolite NaY-supported $Ir(CO)_2$(acac) in CO at 40 °C (2117(w), 2070(s), 2032(m, sh) cm^{-1}).[7] These results suggest that the metal carbonyl species were predominantly $Ir_4(CO)_{12}$.

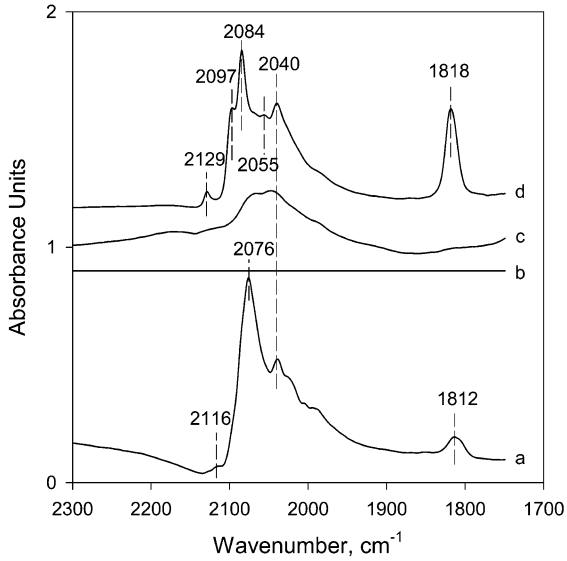

Figure 1. IR spectra characterizing sample made from $Ir_4(CO)_{12}$ and zeolite NaY: (a) $Ir_4(CO)_{12}$ sorbed on the outer surface of the zeolite; (b) the same sample after decarbonylation in He at 300 °C for 4 h; (c) after recarbonylation in CO at 40 °C for 20 h; and (d) after additional treatment in CO at 125 °C for 4 h.

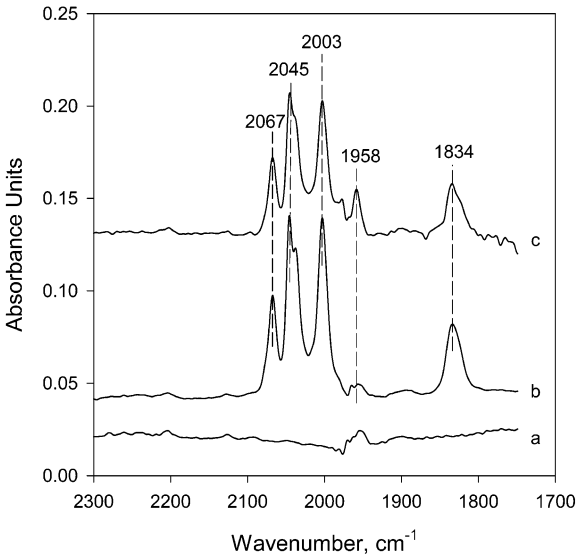

Figure 2. IR spectra of solutions: (a) [PPN][Cl] in THF; (b) $Ir_4(CO)_{12}$ with [PPN][Cl] in THF; and (c) extract formed from $Ir_4(CO)_{12}$ deposited directly on zeolite NaY (the extract solution was [PPN][Cl] in THF).

Extraction of the iridium carbonyl species from the zeolite into [PPN][Cl] in THF resulted in a light-brown colored solution. The IR spectrum (Figure 2c), with ν_{CO} bands at 2067, 2045, 2003, 1958, and 1834 cm^{-1}, nearly matches that of a solution prepared from $Ir_4(CO)_{12}$ and [PPN][Cl] in THF, which shows ν_{CO} bands at 2067, 2045, 2003, 1956 (not marked), and 1834 cm^{-1} (Figure 2b). This result is consistent with the inference that $Ir_4(CO)_{12}$ had been present on the outside surface of the zeolite and was extracted into solution, where it reacted with [PPN][Cl].

TABLE 2: EXAFS Results Characterizing Samples Formed by Treatment of $Ir_4(CO)_{12}$ Deposited Directly on Zeolite NaY[a]

treatment conditions	shell	EXAFS parameters				EXAFS reference	supported species modeled as
		N	*R* [Å]	$10^3\Delta\sigma^2$ [Å^2]	ΔE_0 [eV]		
no treatment	Ir−Ir	2.7 ± 0.1	2.68 ± 0.01	2.7 ± 0.2	−2.4 ± 0.4	Ir−Ir	$Ir_4(CO)_{12}$
	Ir−O_s	0.6 ± 0.1	2.03 ± 0.03	9.0 ± 2.8	0.1 ± 1.7	Pt−O	
	Ir−CO						
	Ir−C_t	2.9 ± 0.1	1.85 ± 0.01	3.0 ± 0.6	0.1 ± 0.2	Ir−C	
	Ir−O*	3.0 ± 0.1	3.01 ± 0.01	3.0 ± 0.4	−0.1 ± 0.2	Ir−O*	
He, 300 °C, 4 h	Ir−Ir (1st-shell)	6.4 ± 0.4	2.65 ± 0.01	7.7 ± 0.5	−4.0 ± 0.3	Ir−Ir	Ir clusters with average diameter of about 11 Å
	Ir−Ir (2nd-shell)	1.0 ± 0.3	3.76 ± 0.02	5.5 ± 2.4	−3.0 ± 1.5	Ir−Ir	
	Ir−$O_{support}$						
	Ir−O_s	1.5 ± 0.1	2.05 ± 0.01	4.1 ± 0.9	0.5 ± 0.7	Pt−O	
	Ir−O_l	1.0 ± 0.1	2.88 ± 0.02	9.0 ± 4.0	4.2 ± 1.5	Pt−O	
CO, 40 °C, 20 h	Ir−Ir	5.9 ± 0.2	2.69 ± 0.01	5.8 ± 0.2	−5.5 ± 0.2	Ir−Ir	Ir clusters with average diameter of about 10 Å
	Ir−Ir (2nd-shell)	1.0 ± 0.2	3.78 ± 0.01	3.0 ± 1.5	3.0 ± 1.7	Ir−Ir	
	Ir−O_s	0.9 ± 0.1	2.13 ± 0.02	8.0 ± 3.2	1.0 ± 1.0	Pt−O	
	Ir−CO						
	Ir−C_t	1.4 ± 0.1	1.84 ± 0.01	3.8 ± 1.6	0.0 ± 0.5	Ir−C	
	Ir−O*	1.0 ± 0.1	2.99 ± 0.01	5.5 ± 1.6	−2.0 ± 0.4	Ir−O*	
CO, 125 °C, 4 h	Ir−Ir	4.2 ± 0.1	2.69 ± 0.01	4.4 ± 0.2	−6.0 ± 0.3	Ir−Ir	$Ir_6(CO)_{16}$
	Ir−O_s	0.6 ± 0.1	2.14 ± 0.01	0.5 ± 1.7	−8.0 ± 0.8	Pt−O	
	Ir−CO						
	Ir−C_t	2.1 ± 0.1	1.88 ± 0.01	5.0 ± 1.0	−5.0 ± 0.6	Ir−C	
	Ir−C_b	1.1 ± 0.2	2.20 ± 0.02	7.0 ± 2.3	−1.0 ± 0.7	Ir−C	
	Ir−O*	1.6 ± 0.1	2.91 ± 0.01	10.0 ± 1.4	0.8 ± 0.5	Ir−O*	
	Ir−Ir (2nd-shell)	1.1 ± 0.2	3.82 ± 0.01	3.0 ± 1.2	−5.6 ± 1.1	Ir−Ir	

[a] Notation: *N*, coordination number; *R*, distance between absorber and backscatterer atoms; $\Delta\sigma^2$, Debye−Waller factor; ΔE_0, inner potential correction; the subscripts s and l refer to short and long, respectively.

EXAFS Evidence of $Ir_4(CO)_{12}$ Deposited on Zeolite NaY. EXAFS data at the Ir L_{III} edge characterizing $Ir_4(CO)_{12}$ supported directly on zeolite NaY are shown in Figures 3a and 4a, and the parameters determined by the data fitting are summarized in Table 2. The EXAFS data (Figure 3a) show oscillations up to a value of *k*, the wave vector, of about 15 Å^{-1}, indicating the presence of near-neighbor high-atomic-weight backscatterers near the Ir absorber atoms. There was no evidence in the Fourier transform (Figure 4a) of higher-shell Ir−Ir contributions.

The errors shown in Table 2 were estimated with the software XDAP;[20,21] these represent precisions, not accuracies. The accuracies are estimated to be as follows: coordination number (*N*), Ir−Ir, ±20%, and Ir−$O_{support}$, ±30%; distance (*R*), Ir−Ir, ±1% and Ir−C and Ir−O, ±2%; Debye−Waller factor ($\Delta\sigma^2$), ±30%; and inner potential correction (ΔE_0), ±10%. The number of parameters used to fit the data in this main-shell analysis, *n*, was 16; the statistically justified number is approximately 40, estimated from the Nyquist theorem,[22] $n = (2\Delta k\Delta r/\pi) + 1$, where Δk and Δr respectively are the *k* and *r* (the metal−backscatterer distance) ranges used in the forward and inverse Fourier transformations ($\Delta k = 12.2$ Å^{-1}, $\Delta r = 5.0$ Å).

Crystallographic data characterizing $Ir_4(CO)_{12}$ show that each Ir atom is bonded to three other Ir atoms (the coordination number is 3), at an average distance of 2.69 Å, with each Ir atom having 3 terminal carbonyl ligands, with average Ir−C and Ir−O* distances of 1.87 and 3.01 Å, respectively.[17] Consistent with these results, the EXAFS data characterizing $Ir_4(CO)_{12}$ directly deposited on zeolite NaY (Table 2) indicate an Ir−Ir coordination number of 2.7, at an average distance of 2.68 Å; the Ir−C_t (where C_t represents terminal carbon) and Ir−O* coordination numbers, 2.9 and 3.0, respectively, also agree, within the expected error, with the values representing crystalline $Ir_4(CO)_{12}$.

IR Spectra Characterizing Attempted Recarbonylation of Decarbonylated $Ir_4(CO)_{12}$ Deposited on Zeolite NaY. The sample was decarbonylated by treatment in flowing He at 300 °C for 4 h. The IR spectrum (Figure 1b), measured after the sample had been cooled to room temperature, has no peaks in the carbonyl stretching frequency range, indicating complete decarbonylation of the iridium.

This sample was recarbonylated in flowing CO at 40 °C for 20 h. The resultant spectrum (Figure 1c) includes very broad ν_{CO} bands of low intensity, not resembling the spectrum of $Ir_4(CO)_{12}$, which evidently was not reformed.

After this decarbonylated sample had been treated in CO at a higher temperature (125 °C) for 1 h, the resultant spectrum was found to include ν_{CO} bands at 2129, 2097, 2084, 2055, 2040, and 1818 cm^{-1}. The intensities of these bands increased for 4 h of CO treatment at 125 °C (Figure 1d). The spectrum is almost the same as that of the isomer of $Ir_6(CO)_{16}$ with edge-bridging ligands (ν_{CO}: 2129, 2096, 2084, 2054, 2039, and 1818 cm^{-1}), which is reported to have been synthesized from $Ir(CO)_2$(acac) in zeolite NaY in flowing CO at 125 °C.[23]

EXAFS Results Characterizing Decarbonylation and Attempted Recarbonylation of $Ir_4(CO)_{12}$ Deposited on Zeolite NaY. The EXAFS parameters (Table 2) characterizing the decarbonylated sample formed by direct deposition of $Ir_4(CO)_{12}$ on the zeolite were analyzed by a method similar to that stated above for the sample before decarbonylation. The Ir−Ir (first-shell and second-shell) and two Ir−$O_{support}$ contributions were added to represent the overall fit of the data (Figures 3b and 4b). The number of parameters used to fit the data in this EXAFS analysis was 16; the statistically justified number was approximately 40. The Ir−Ir first-shell and second-shell coordination numbers, 6.4 and 1.0, respectively, indicate iridium clusters of roughly 20 atoms each, on average. Such clusters are approximately 11 Å in average diameter,[24] indicating that some aggregation accompanied the decarbonylation of the iridium.

The EXAFS data charactering the product of the attempted recarbonylation of the decarbonylated sample in CO at 40 °C for 20 h are summarized in Table 2 and in Figures 3c and 4c. The Ir−Ir first-shell and second-shell coordination numbers, 5.9 and 1.0, respectively, were still high in comparison with those representing $Ir_4(CO)_{12}$, and the sample is inferred to have

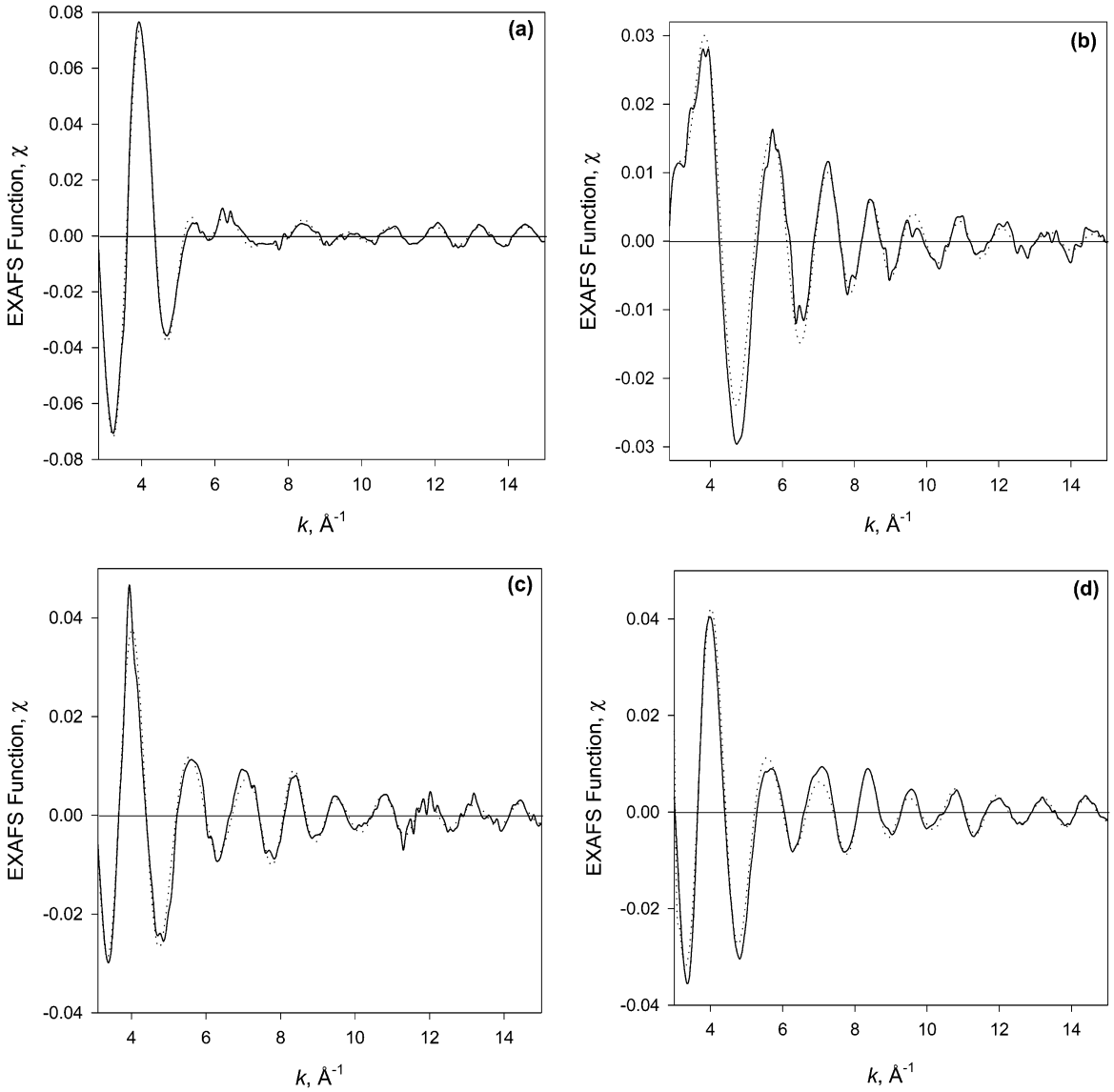

Figure 3. Results of EXAFS analysis for $Ir_4(CO)_{12}$ directly deposited on zeolite NaY: experimental EXAFS function (solid line) and sum of all of the calculated contributions (dotted line). (a) Sample before treatment; (b) after decarbonylation in He 300 °C for 4 h; (c) after treatment in CO 40 °C for 20 h; and (d) after treatment in CO 125 °C for 4 h.

contained iridium clusters of roughly 20 atoms each, on average.[24] Thus, the data indicate that the treatment in CO at 40 °C hardly changed the size of the iridium clusters.

Ir−CO contributions were also observed (Table 2). The Ir−C_t and Ir−O* coordination numbers, 1.4 and 1.0, respectively, are consistent with CO adsorption on the iridium clusters, but they provide almost no structural insights about the bonding of the CO.

In contrast to the sample treated in CO at 40 °C, that treated in CO at 125 °C (for 4 h) underwent significant changes in the cluster frame (Table 2). The EXAFS data representing this sample (Figures 3d and 4d) were analyzed to account for both Ir−C_t and Ir−C_b contributions (the subscript b refers to bridging). (In contrast, Ir−C_b contributions were not evident in the analysis for the sample treated in CO at 40 °C, represented as $Ir_4(CO)_{12}$; only terminal carbonyl contributions were indicated by the data, and only terminal carbonyl ligands are present in $Ir_4(CO)_{12}$.) The Ir−Ir second shell was also accounted for in the analysis. Thus, the number of parameters used to fit the data in this analysis was 24; the statistically justified number was again approximately 40. The Ir−Ir first- and second-shell coordination numbers, 4.2 and 1.1, respectively, correspond to an octahedral Ir_6 frame, as in $Ir_6(CO)_{16}$.[25] The Ir−C_t and Ir−C_b coordination numbers, 2.1 and 1.1, respectively, nearly match those representing the isomer of $Ir_6(CO)_{16}$ with edge-bridging CO ligands, which has Ir−C_t and Ir−C_b coordination numbers of 2.0 and 1.3, respectively.[25] Because the terminal and bridging carbonyl oxygen atoms are located at nearly the same distance from the absorber Ir atom, it is difficult to separate the two contributions and to determine the overall Ir−O* coordination number. Thus, the difference between the Ir−O* coordination number, 1.6, and the expected coordination number, 3.3, is inferred to be a result of there being two types of carbonyl oxygen contributions at the same distance but experiencing different degrees of multiple scattering that lead to different phase shifts, which may give a negative interference and a low estimate of the overall coordination number.[13] The data thus are inferred to be consistent with the isomer of $Ir_6(CO)_{16}$ with both edge-bridging and terminal CO ligands (Figure 5), consistent with the IR spectra.

IR Evidence of $Ir_4(CO)_{12}$ Formed in Zeolite NaY. $Ir(CO)_2$-(acac) in *n*-pentane solution was brought in contact with the calcined zeolite NaY support, and after removal of the solvent, the solid was beige in color and had an IR spectrum (Figure

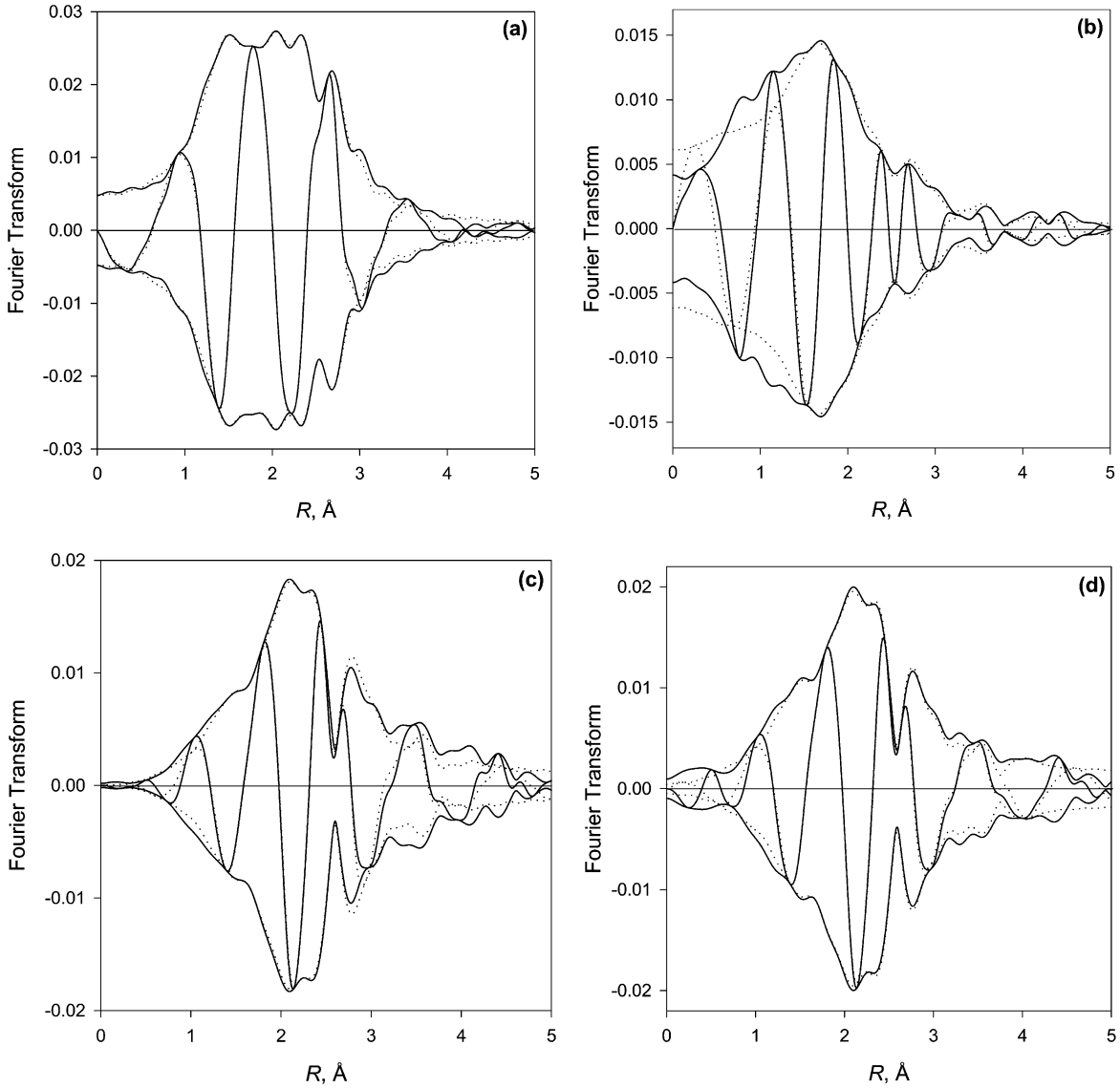

Figure 4. Results of EXAFS analysis for sample containing $Ir_4(CO)_{12}$ directly deposited on zeolite NaY: imaginary part and magnitude of uncorrected Fourier transform (k^0 weighted, $\Delta k = 2.8-15.0$ Å^{-1}) of experimental EXAFS (solid line) and sum of the calculated contributions (dotted line). (a) Sample as is; (b) after decarbonylation in He 300 °C for 4 h; (c) after subseqeunt treatment in CO at 40 °C for 20 h; and (d) after subsequent treatment in CO 125 °C for 4 h.

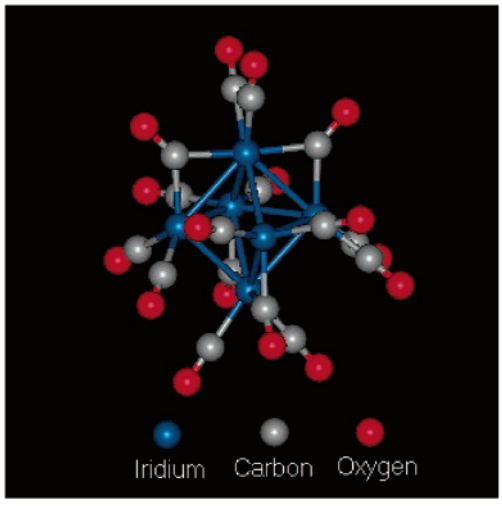

Figure 5. Structure of the isomer of $Ir_6(CO)_{16}$ with edge bridging and terminal CO ligands

6a) with two strong ν_{CO} bands, at 2082 and 1995 cm^{-1}, indicating an iridium dicarbonyl species.[7] Treatment of this sample in flowing CO at 40 °C for 12 h led to a light-brown colored solid, with an IR spectrum (ν_{CO}: 2116 w, 2072 s, 2040 s cm^{-1}) resembling that of $Ir_4(CO)_{12}$ supported on zeolite NaY.[7] The band intensities did not change after an additional 8 h of treatment (Figure 6b).

Attempts to extract this iridium carbonyl from the zeolite with [PPN][Cl] in THF were not successful (although $Ir_4(CO)_{12}$ is slightly soluble in THF and even more soluble in [PPN][Cl]/THF mixtures). The supernatant solution had no IR absorptions in the ν_{CO} region. This result is consistent with previous work.[7,23] We infer that the iridium carbonyls were trapped in the zeolite supercages, consistent with the diameter of $Ir_4(CO)_{12}$, approximately 9 Å; $Ir_4(CO)_{12}$ is small enough to fit in the supercage (12.5 Å in diameter) but too large to fit easily through the windows (7.4 Å in diameter).

EXAFS Evidence of $Ir_4(CO)_{12}$ Formed in Zeolite NaY. The EXAFS results characterizing $Ir_4(CO)_{12}$ formed by reductive carbonylation of sorbed $Ir(CO)_2(acac)$ in zeolite NaY are summarized in Table 3. The Ir−Ir, Ir−$O_{support}$, and two Ir−CO contributions were added to represent the overall fit of the data representing the sample before decarbonylation. There was no

TABLE 3: EXAFS Results Characterizing Samples Formed by Treatment of $Ir(CO)_2(acac)$ Sorbed in Zeolite NaY[a]

treatment conditions	shell	EXAFS parameters				EXAFS reference	supported species modeled as
		N	R [Å]	$10^3\Delta\sigma^2$ [Å^2]	ΔE_0 [eV]		
CO, 40 °C, 20 h	Ir−Ir	2.7 ± 0.1	2.70 ± 0.01	4.0 ± 0.1	−6.8 ± 0.1	Ir−Ir	$Ir_4(CO)_{12}$
	$Ir-O_s$	0.9 ± 0.1	2.12 ± 0.01	0.0 ± 0.3	−3.0 ± 0.3	Pt−O	
	Ir−CO						
	$Ir-C_t$	3.0 ± 0.1	1.84 ± 0.01	5.0 ± 0.1	6.4 ± 0.1	Ir−C	
	Ir−O*	1.9 ± 0.1	2.97 ± 0.01	0.8 ± 0.1	2.0 ± 0.1	Ir−O*	
He, 300 °C, 4 h	Ir−Ir	2.9 ± 0.2	2.66 ± 0.01	5.3 ± 0.4	−0.0 ± 1.1	Ir−Ir	Ir_4
	$Ir-O_{support}$						
	$Ir-O_s$	1.2 ± 0.1	2.15 ± 0.01	1.0 ± 0.9	−1.0 ± 0.7	Pt−O	
	$Ir-O_l$	0.7 ± 0.1	2.63 ± 0.01	3.0 ± 3.0	−9.5 ± 0.7	Pt−O	

[a] Notation as in Table 1.

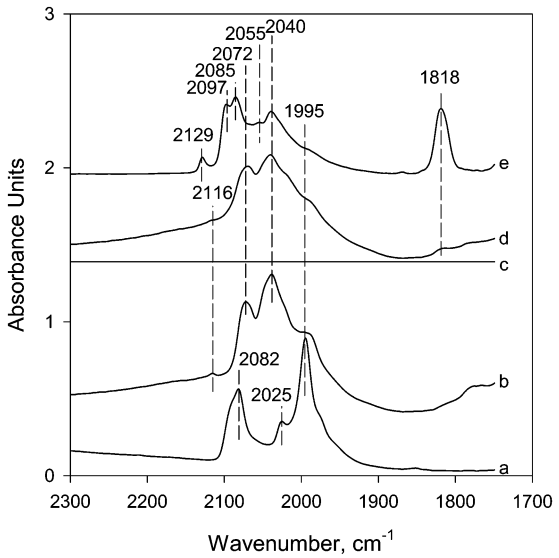

Figure 6. IR spectra characterizing the sample prepared from $Ir(CO)_2$-(acac) and zeolite NaY: (a) $Ir(CO)_2(acac)$ sorbed in zeolite NaY; (b) sample after treatment in CO at 40 °C for 20 h; (c) after decarbonylation in He at 300 °C for 4 h; (d) after recarbonylation in CO at 40 °C for 20 h; and (e) after additional treatment in CO at 125 °C for 4 h.

evidence of higher-shell Ir−Ir contributions. The number of parameters used to fit the data in this analysis was 16; the statistically justified number was approximately 40. The Ir−Ir coordination number, 2.7, matches the crystallographically determined Ir−Ir first-shell coordination number of $Ir_4(CO)_{12}$ (3.0) within expected error. Similarly, the $Ir-C_t$ coordination number determined from the EXAFS data, 3.0, also matches the crystallographic value. The Ir−O* coordination number, 1.9, however, is less than the crystallographic value of 3. This discrepancy is in part a consequence of the relatively large uncertainties in the Ir-low-Z parameters (± 50% for coordination numbers; ± 10% for distances)[26] and in part can be explained on the basis of multiple scattering effects. (In metal carbonyls with terminal CO ligands, the metal is in an almost linear array with the C and O atoms of the ligands; the EXAFS analysis is not straightforward because the multiple scattering effect is prominent.[27,28]) We infer that the iridium was predominately present as $Ir_4(CO)_{12}$, consistent with the IR data.

After decarbonylation of the sample consisting of $Ir_4(CO)_{12}$ in the zeolite in He at 300 °C for 4 h, it became gray in color, and the resulting IR spectrum (Figure 6c) included no ν_{CO} bands. These results show that the clusters were fully decarbonylated.

In the analysis of the EXAFS data representing the sample formed by decarbonylation of the zeolite-encaged $Ir_4(CO)_{12}$ at 300 °C, the Ir−Ir and two $Ir-O_{support}$ contributions were added to represent the overall fit of the data. There was no evidence of higher-shell Ir−Ir contributions. The number of parameters used to fit the data in this first-shell analysis was 12; the statistically justified number was again approximately 40. The Ir−Ir coordination number, 2.9, indicates that the decarbonylated clusters can be modeled as Ir_4 tetrahedra. Such clusters have been reported to have formed similarly on other supports.[11,29]

Recarbonylation of Decarbonylated $Ir_4(CO)_{12}$. Recarbonylation of this decarbonylated sample in flowing CO at 40 °C for 20 h gave a sample with an IR spectrum (Figure 6d) closely resembling that of Figure 6b, indicating that $Ir_4(CO)_{12}$ was reformed, consistent with earlier results.[8,23] Further treatment of this sample in CO at 125 °C for 4 h, gave the IR spectrum shown in Figure 6e (ν_{CO}: 2129, 2097, 2085, 2040, and 1818 cm^{-1}). A comparison of this spectrum with that shown in Figure 1d indicates that, although the intensities are slightly different, the sample is characterized by the same CO frequencies, and the spectrum is similar to that previously attributed to the isomer of $Ir_6(CO)_{16}$ with edge-bridging CO ligands in zeolite NaY.[23]

Our results are consistent with previous work[23,30] indicating that $Ir_4(CO)_{12}$ and $Ir_6(CO)_{16}$ in zeolite NaY can be reformed by recarbonylation of Ir_4 in CO at 40 °C and 125 °C, respectively.

Discussion

The EXAFS results (Table 2) characterizing the iridium clusters deposited on the outside surface of the zeolite indicate that, on average, they consisted of about 20 atoms each and were about 11 Å in diameter. The SEM data show that the external surface area of the zeolite crystals was roughly 8 m^2/g (we approximate the particles as spheres), so that the loading of $Ir_4(CO)_{12}$ was about 0.7 molecules per nm^2. Thus, as the diameter of a molecule of $Ir_4(CO)_{12}$ is about 0.9 nm, the coverage of the outer zeolite surface with $Ir_4(CO)_{12}$ was approximately a monolayer. We suggest that the aggregation of the clusters during decarbonylation was facilitated by their nearness to each other.

After recarbonylation at 40 °C, the aggregated iridium clusters were characterized by an IR spectrum (Figure 1c) with very broad ν_{CO} bands of low intensity. This spectrum is similar to that reported for CO adsorbed on metallic iridium particles supported on alumina[31] and does not resemble the spectra of molecular clusters such as $Ir_4(CO)_{12}$ or $Ir_6(CO)_{16}$. The EXAFS data show only a little change in the Ir−Ir first-shell coordination number as a result of the recarbonylation (Table 2), and we infer that the bonding of CO to the iridium was at least roughly comparable to the chemisorption of CO on small metallic iridium particles.[31]

In contrast, when the decarbonylated sample was treated in CO at a higher temperature, 125 °C, the IR spectrum (Figure 1d) was characterized by ν_{CO} bands similar to those of $Ir_6(CO)_{16}$,[23] and the EXAFS parameters indicating Ir−Ir first- and second-shell coordination numbers 4.2 and 1.1, respectively, also point to hexairidium clusters. The formation of molecular

$Ir_6(CO)_{16}$ clusters from clusters that had, on average, higher nuclearities, implies that the larger clusters were fragmented as a result of the treatment in CO, presumably being converted into mononuclear iridium carbonyl species, which subsequently assembled into molecules of $Ir_6(CO)_{16}$. The observations are similar to those reported by several researchers. For example, Beutel et al.[23] observed that small Ir_4 clusters in zeolite NaY were oxidatively fragmented in the presence of CO at low temperatures and were assembled to give $Ir_6(CO)_{16}$ as the temperature was raised to 125 °C. Serykh et al.[32] reported platinum cluster anions in zeolite X that could be almost reversibly decarbonylated and recarbonylated. van't Blik et al.[33] observed that during the adsorption of CO on small clusters of alumina-supported rhodium, the metal−metal bonds were broken to give mononuclear metal complexes incorporating Rh(I), in a process that is described as an oxidative fragmentation.[33,34] (These authors did not treat their sample to reform rhodium clusters.) Smith et al.[35] similarly observed that $Rh_6(CO)_{16}$ could be oxidized on alumina when the water content was high, resulting in a mononuclear Rh(I) carbonyl species, and they reformed $Rh_6(CO)_{16}$ on their support from the mononuclear fragments with CO at 25 °C and inferred that the process involves water or surface OH groups. Similarly, Bergeret et al.[36] observed that the adsorption of CO at 27 °C led to a complete disintegration of the rhodium aggregates in zeolite Y, giving monomeric species identified by IR spectroscopy as $Rh^I(CO)_2$. Subsequent treatment of the fragmented species in Bergeret's sample in the presence of a $CO:H_2O$ mixture at 27 °C led to the aggregation of the $Rh^I(CO)_2$ species into metal clusters. Thus, fragmentation can be followed by aggregation on the support surface, depending on the surface composition and reaction conditions. On the basis of these results, we infer that similar chemistry occurred in our sample at 125 °C but that it was too slow to observe at 40 °C; furthermore, we infer that the formation of the metal carbonyl clusters from mononuclear species involved water or OH groups in the zeolite.

In contrast to the slightly oxophilic metals Rh and Ir, more noble metals such as Pd[6,37] and Pt,[38] rather than fragmenting, tend to aggregate more readily to form larger supported clusters in the presence of CO.

The results representing the clusters on the outer surface of the zeolite are contrasted to the results characterizing $Ir_4(CO)_{12}$ entrapped in the zeolite supercages, which show that these clusters could be decarbonylated in the absence of significant fragmentation or aggregation and then recarbonylated at 40 °C to give back $Ir_4(CO)_{12}$ in high yield. Only treatment of this sample in CO at a higher temperature (125 °C) resulted in the formation of larger clusters, $Ir_6(CO)_{16}$. The diameter of this cluster, approximately 11 Å, indicates that it just fits in the zeolite supercage and is too large to fit through the windows connecting them. These results are consistent with earlier observations.[39]

Thus, there is a sharp distinction between the behavior of the clusters in the zeolite cages and those on the outer zeolite surface. Entrapment in the cages hinders the aggregation of the clusters. The stabilization is suggested to be related to the separation of the clusters from each other in the cages (only about 2% of the supercages were occupied by clusters, assuming one cluster per supercage−only one carbonyl cluster fits in a supercage) and the restriction of motion of the clusters between supercages, because they are larger in diameter than the windows connecting the cages.

However, the Ir_4 cluster without CO ligands is only about 6 Å in diameter, and it would easily fit through the windows to undergo aggregation. However, this did not happen, at least under our conditions of decarbonylation (300 °C in He).

Thus, we infer that there is more to the stabilization of clusters in the zeolite than just a geometric effect. EXAFS data characterizing the Ir_4 clusters in the zeolite show an Ir−O distance characteristic of chemical bonds (Table 3), consistent with the literature. Furthermore, calculations at the density functional level indicate that Ir_4 clusters are quite stably bonded to a zeolite.[40] We suggest that the rather strong bonding of the individual clusters to the interior of a zeolite cage hinders their migration and aggregation. We emphasize that at high temperatures these cluster−support bonds break and aggregation occurs.[2,41,42]

In summary, the results presented here show that zeolite cages help to minimize the migration and aggregation of metal clusters in them, and this stabilization of the metal dispersion contributes to the usefulness of zeolites as supports for metal catalysts.

The literature[43,44] indicates a potential application of zeolite-supported iridium catalysts for selective ring opening of naphthenic molecules. The authors[44] referred to regeneration of their catalysts by burning of coke deposits at high temperature, but they did not mention that redispersion of the iridium is part of their overall catalyst regeneration process. Our data suggest that it might be feasible to regenerate their catalysts by treating them in CO to give oxidatively fragmented species that could then be converted into small iridium carbonyl clusters and then decarbonylated iridium clusters.

Conclusions

Zeolite-supported $Ir_4(CO)_{12}$ was synthesized by deposition on the outer surfaces of crystallites of zeolite NaY and alternatively by carbonylation of sorbed $Ir(CO)_2(acac)$ in the cages of the zeolite. The iridium clusters residing on the outer surface of the zeolite are easily aggregated under decarbonylation conditions (He flow, 300 °C) and are not reversibly recarbonylated. In contrast, when the clusters are trapped in the cages of the zeolite, they are more stably dispersed and can be reversibly recarbonylated to give back Ir_4 clusters.

Acknowledgment. This research was supported by the U.S. Department of Energy, Office of Energy Research, Office of Basic Energy Sciences, Division of Chemical Sciences, Contract FG02-87ER13790. EXAFS experiments were done at the Stanford Synchrotron Radiation Laboratory (SSRL, beam line 4-1b), which is operated by the Department of Energy, Office of Basic Energy Sciences, and at the National Synchrotron Light Source (NSLS, beam line X-11A). The NSLS is supported by the Department of Energy, Division of Materials Sciences and Division of Chemical Sciences, under Contract No. DE-AC02-76CH00016. We thank the staffs of these beam lines for their assistance. The EXAFS data were analyzed with the software XDAP.[20]

Supporting Information Available: A SEM image of the zeolite crystallites used in the synthesis.[21] This material is available free of charge via the Internet at http://pubs.acs.org.

References and Notes

(1) Miller, J. T.; Agrawal, N. G. B.; Lane, G. S.; Modica, F. S. *J. Catal.* **1996**, *163*, 106.

(2) Jacobs, P. A. *Stud. Surf. Sci. Catal.* **1986**, *29*, 357.

(3) (a) Jaeger, N. I.; Moeller, K.; Plath, P. J. *Z. Naturforsch. A* **1981**, *36A*, 1012. (b) Schulz-Ekloff, G. Metal Clusters in Zeolites. In *Comprehensive Supramolecular Chemistry*; Atwood, J. L., et al., Eds.; Pergamon: Oxford 1996; p 549, Vol 7.

(4) Ichikawa, M. *Adv. Catal.* **1992**, *38*, 283.

(5) Kawi, S.; Gates, B. C. In *Clusters and Colloids from Theory to Applications*; Schmid, G., Ed.; VCH:; Weinheim, 1994; p 299.
(6) Sachtler, W. M. H.; Zhang, Z. *Adv. Catal.* **1993**, *39*, 129.
(7) Kawi, S.; Gates, B. C. *Catal. Lett.* **1991**, *10*, 263.
(8) Kawi, S.; Chang, J. R.; Gates, B. C. *J. Am. Chem. Soc.* **1993**, *115*, 4830.
(9) Alexeev, O.; Panjabi, G.; Gates, B. C. *J. Catal.* **1998**, *173*, 196.
(10) Zhao, A.; Gates, B. C. *J. Am. Chem. Soc.* **1996**, *118*, 2458.
(11) Weber, W. A.; Gates, B. C. *J. Phys. Chem. B* **1997**, *101*, 10423.
(12) Kawi, S.; Chang, J. R.; Gates, B. C. *J. Phys. Chem.* **1993**, *97*, 10599.
(13) Maloney, S. D.; Kelley, M. J.; Koningsberger, D. C.; Gates, B. C. *J. Phys. Chem.* **1991**, *95*, 9406.
(14) Wyckoff, R. W. G. *Crystal Structures*, 2nd ed.; Wiley: New York, 1963; Vol. 1, p 10.
(15) Troemel, M.; Lupprich, E. *Z. Anorg. Chem.* **1975**, *414*, 160.
(16) Duivenvoorden, F. B. M.; Koningsberger, D. C.; Uh, Y. S.; Gates, B. C. *J. Am. Chem. Soc.* **1986**, *108*, 6254.
(17) Churchill, M. R.; Hutchinson, J. P. *Inorg. Chem.* **1978**, *17*, 3528.
(18) Koningsberger, D. C. In *Synchrotron Techniques in Interfacial Electrochemistry*; Melendres, C. A., Tadjeddine, A., Eds.; Kluwer: Dordrecht, 1994; p 181.
(19) Alexeev, O. S.; Graham, G. W.; Shelef, M.; Adams, R. D.; Gates, B. C. *J. Phys. Chem. B* **2002**, *106*, 4697.
(20) Vaarkamp, M. *Catal. Today* **1998**, *39*, 271.
(21) Vaarkamp, M.; Linders, J. C.; Koningsberger, D. C. *Physica B* **1995**, *208 & 209*, 159.
(22) Koningsberger, D. C.; Prins, R.; Editors *X-ray Absorption: Principles, Applications, Techniques of EXAFS, SEXAFS, and XANES*; Wiley: New York, 1988; p 395.
(23) Beutel, T.; Kawi, S.; Purnell, S. K.; Knözinger, H.; Gates, B. C. *J. Phys. Chem.* **1993**, *97*, 7284.
(24) Kip, B. J.; Duivenvoorden, F. B. M.; Koningsberger, D. C.; Prins, R. *J. Catal.* **1987**, *105*, 26.
(25) Garlaschelli, L.; Martinengo, S.; Bellon, P. L.; Demartin, F.; Manassero, M.; Chiang, M. Y.; Wei, C. Y.; Bau, R. *J. Am. Chem. Soc.* **1984**, *106*, 6664.
(26) Weber, W. A.; Zhao, A.; Gates, B. C. *J. Catal.* **1999**, *182*, 13.
(27) Van Zon, F. B. M.; Kirlin, P. S.; Gates, B. C.; Koningsberger, D. C. *J. Phys. Chem.* **1989**, *93*, 2218.
(28) Teo, B.-K. *J. Am. Chem. Soc.* **1981**, *103*, 3990.
(29) Kawi, S.; Gates, B. C. *J. Phys. Chem.* **1995**, *99*, 8824.
(30) Kawi, S.; Gates, B. C. *J. Chem. Soc., Chem. Commun.* **1991**, 994.
(31) McVicker, G. B.; Baker, R. T. K.; Garten, R. L.; Kugler, E. L. *J. Catal.* **1980**, *65*, 207.
(32) Serykh, A. I.; Tkachenko, O. P.; Borovkov, V. Yu.; Kazansky, V. B.; Beneke, M.; Jaeger, N. I.; Schulz-Ekloff, G. *Phys. Chem. Chem. Phys.* **2000**, *2*, 5647.
(33) van't Blik, H. F. J.; van Zon, J. B. A. D.; Huizinga, T.; Vis, J. C.; Koningsberger, D. C.; Prins, R. *J. Am. Chem. Soc.* **1985**, *107*, 3139.
(34) Lamb, H. H.; Gates, B. C.; Knözinger, H. *Angew. Chem.* **1988**, *100*, 1162.
(35) Smith, A. K.; Hugues, F.; Theolier, A.; Basset, J. M.; Ugo, R.; Zanderighi, G. M.; Bilhou, J. L.; Graydon, W. F. *Inorg. Chem.* **1979**, *18*, 3104.
(36) Bergeret, G.; Gallezot, P.; Gelin, P.; Ben Taarit, Y.; Lefebvre, F.; Naccache, C.; Shannon, R. D. *J. Catal.* **1987**, *104*, 279.
(37) Anderson, S. L.; Mizushima, T.; Udagawa, Y. *J. Phys. Chem.* **1991**, *95*, 6603.
(38) Chang, J. R.; Koningsberger, D. C.; Gates, B. C. *J. Am. Chem. Soc.* **1992**, *114*, 6460.
(39) Labouriau, A.; Panjabi, G.; Enderle, B.; Pietrass, T.; Gates, B. C.; Earl, W. L.; Ott, K. C. *J. Am. Chem. Soc.* **1999**, *121*, 7674.
(40) Ferrari, A. M.; Neyman, K. M.; Mayer, M.; Staufer, M.; Gates, B. C.; Rösch, N. *J. Phys. Chem. B* **1999**, *103*, 5311.
(41) Busch, F.; Jaeger, N.; Schulz-Ekloff, G.; Schnell, R.; Klein, H.; Füss, H. *Zeolites* **1996**, *17*, 244.
(42) Busch, F.; Jaeger, N. I.; Schulz-Ekloff, G.; Tkachenko, O. P.; Shpiro, E. S. *J. Chem. Soc., Faraday Trans.* **1996**, *92*, 693.
(43) McVicker, G. B.; Daage, M.; Touvelle, M. S.; Hudson, C. W.; Klein, D. P.; Baird, W. C., Jr.; Cook, B. R.; Chen, J. G.; Hantzer, S.; Vaughan, D. E. W.; Ellis, E. S.; Feeley, O. C. *J. Catal.* **2002**, *210*, 137.
(44) Touvelle, M. S.; Klein, D. P.; Chen, T.-J.; Martens, L. R.; Ellis, E. S. WO A1 0208364, 20020131; *PCT Int. Appl.* 32 pp.